Corrosion Science 50 (2008) 2456–2464

Contents lists available at ScienceDirect

Corrosion Science

journal homepage: www.elsevier.com/locate/corsci

The effect of pre-corrosion and steel microstructure on inhibitor performance in CO_2 corrosion

L.D. Paolinelli [a], T. Pérez [b], S.N. Simison [a,*]

[a] División Corrosión – INTEMA, UNMdP, Ave. Juan B. Justo 4302, B7608FDQ, Mar del Plata, Argentina
[b] Centro de Investigaciones Industriales (CINI), Simini 250, 2804 Campana, Argentina

ARTICLE INFO

Article history:
Received 4 June 2007
Accepted 17 June 2008
Available online 4 July 2008

Keywords:
A. Carbon steel
B. EIS
C. CO_2 corrosion
C. Steel microstructure
C. Imidazolines

ABSTRACT

The importance of chemical composition and microstructure on CO_2 corrosion of carbon and low alloy steels has been widely recognized, still contradictory results can be found in the literature. The aim of this work is to assess the relationship between microstructure, surface condition and inhibitor efficiency in CO_2 corrosion. A C–Mn steel with two different microstructures was tested in a deoxygenated 5% wt. NaCl solution saturated with CO_2 at 40 °C, pH 6. A commercial imidazoline-based inhibitor was added after different pre-corrosion periods. The results obtained showed that pre-corrosion decreases the inhibitor efficiency, but that its impact is microstructure dependent.

1. Introduction

The widespread use of carbon and low alloyed steels in the petroleum industry is primarily due to economic reasons. Nevertheless, their corrosion resistance is limited in certain oil and gas environments with high chloride and carbon dioxide concentrations. Depending on their chemical composition and manufacturing processes, carbon and low alloyed steels may have different microstructures which influence their mechanical properties and corrosion resistance.

CO_2 corrosion, usually referred to as sweet corrosion, is one of the most severe forms of attack in the oil and gas production and transportation [1,2].

CO_2 dissolves in water giving carbonic acid which is dissociated, decreasing the solution pH.

It is widely known that CO_2 increases the corrosion rate of C–Mn and low alloy steels mainly because of its effect on hydrogen evolution reaction [3,4].

In pH > 4 solutions, the H^+ concentration is small so H_2CO_3 presence allows for higher reduction rates, and therefore increases the corrosion rate.

There is a possibility of H_2CO_3 and HCO_3^- direct reduction according to these equations [5]:

$$2H_2CO_3 + 2e^- \rightarrow H_2 + 2HCO_3^- \quad (1)$$

$$E^0 = -0.622\ \text{V (SCE)}$$

$$2HCO_3^- + 2e^- \rightarrow H_2 + 2CO_3^{2-} \quad (2)$$

$$E^0 = -0.856\ \text{V (SCE)}$$

At pH > 5, the direct reduction of bicarbonate ion can become meaningful as its concentration increases with pH.

The dominant anodic reaction in CO_2 corrosion is the electrochemical dissolution of iron into ferrous ion.

As a consequence of corrosion processes, a layer of corrosion products is formed on the surface of the steel. Its protection properties depend on the environmental conditions as well as on the characteristics of the material. The presence of iron carbonate ($FeCO_3$) is commonly related with the formation of protective layers [6–11]. Because of its low solubility (pK_{sp} = 10.54 at 25 °C [12]), $FeCO_3$ precipitates when ferrous cations (Fe^{2+}) interact with carbonate (CO_3^{2-}) and bicarbonate (HCO_3^-) ions in the solution. The surface scales formed below 40 °C in chloride media containing carbon dioxide consist mainly of cementite (Fe_3C) with some $FeCO_3$ and steel alloying elements [1]. Fe_3C is part of the original steel microstructure and accumulates on the surface after the preferential dissolution of ferrite (α-Fe) into Fe^{2+}. Cementite is said to provide an available area for cathodic reactions and to lead to a galvanic coupling with α-Fe, therefore the characteristics and composition of this surface layer should be determinant for steel performance in CO_2 containing brines [13].

The amount and morphology of cementite in steels relies on the chemical composition and manufacturing processes (heat

* Corresponding author. Tel.: +54 223 4816600; fax: +54 223 4810046.
E-mail address: ssimison@fi.mdp.edu.ar (S.N. Simison).

0010-938X/$ - see front matter © 2008 Elsevier Ltd. All rights reserved.
doi:10.1016/j.corsci.2008.06.031

treatment) undergone, so the microstructure is expected to affect surface scales.

The key part the chemical composition and microstructure play on CO_2 corrosion of carbon and low alloy steels has been widely documented. Still several aspects remain uncertain, and contradictory results can be found in the literature [1,2]. The effect of these variables on corrosion product films formation and their properties as well as on the inhibitors efficiency is far from clear. This could be due to the complexity of the problem itself and to the difficulty implied in the description of the mechanisms involved. Moreover, test conditions also vary in a wide range, rendering the comparison almost impossible.

Whenever the environment is highly aggressive or the scales formed on the steel are non-protective, the use of corrosion inhibitors is a requirement. Organic compounds containing nitrogen such as amines, amides, quaternary ammonium salts and especially imidazolines and their derivatives are commonly employed in the petroleum industry to decrease corrosion rates. They are usually adsorbed on the metallic surface generating a protective film that interferes with the electrochemical reactions involved in the corrosion processes. Despite their extensive use, their action mechanisms remain mostly unknown, and very few studies have taken into consideration the role surface scale properties have on inhibitors efficiency [14–22]. From Rozenfeld et al. [14] results, inhibitors incorporate into the corrosion product layer and form a protective barrier between the base material and the corrosive media. French et al. [15] obtained SEM results which proved that the inhibitors modified the structure of the corrosion product layer. They suggested that, in order to interact with corrosion products, the structure of the inhibitor has to be appropriate, and that some inhibitors can be effective on iron carbonates or sulphides though not on iron oxides. Oblonsky et al. [16] studied the adsorption of octadecyldimethylbenzylammonium chloride (ODBAC) on carbon steel with two different microstructures. They found that ODBAC strongly physisorbs on ferritic–pearlitic microstructures and weakly on martensitic ones. They also put forward that the passive film formed on the martensitic steel is more stable and prevents the optimal adsorption of the inhibitor.

Gulbrandsen et al. [17,18] analyzed the effect of pre-corrosion, steel microstructure and of chemical composition on the inhibition of CO_2 corrosion. They concluded that cathodic inhibition has a decisive influence since the rate of the cathodic reaction controls the corrosion rate. The anodic as well as the cathodic inhibition depend on pre-corrosion time and steel type. They deduced that the negative effect of pre-corrosion is codetermined by the steel microstructure and chemical composition, and by the inhibitor molecular structure. Besides, they observed that the pre-corrosion effect seems to be connected with the presence of a cementite layer on the steel surface.

In previous works, we have shown that the inhibitor efficiency is affected by microstructure, and that the effect could be specific to the inhibitor molecular structure [19–22].

Since the effect of the steel microstructure on the inhibitor performance in CO_2 corrosion remains uncertain, it is important to gain further knowledge on the participating inhibition mechanisms, considering the influence of corrosion products and the steel microstructural components. Because imidazoline derivatives are largely used by the petroleum industry, they were selected for this work. Both EIS and standard DC measurements (E_{corr}, LPR polarization curves) were employed to study the performance of an oleic imidazoline-based inhibitor on a carbon steel with two different microstructures (ferrite–pearlite and tempered martensite) in a high chloride, CO_2 saturated solution. Surface films characteristics were studied by means of SEM.

2. Experimental

A carbon steel with the following composition (wt%): 0.38 C–0.99 Mn– 0.33 Si–0.17 Cr–<0.01 P–<0.01 S was used. Two different heat treatments were conducted on the samples in a lab furnace: annealing (austenized at 890 °C and furnace cooled – FP samples), and quenching and tempering (Q&T) (austenized at 890 °C, water Q&T 1 h at 700 °C – TM samples). Heat treatment conditions were chosen to obtain two very distinct cementite morphologies: coarse laminar and globular (Fig. 1).

Working electrodes were machined from these heat-treated materials into 5 mm diameter bars, cut and mounted with epoxy resin in a disc electrode holder. Electrical contact between the sample and holder was obtained with silver loaded epoxy resin. For the electrochemical tests, surfaces were polished with 600-grit SiC paper, washed with distilled water and rinsed with ethanol.

Experiments were conducted at atmospheric pressure, 40 °C and under low speed magnetic stirring. Three-electrode jacketed test cells with a working volume of 0.5 l and a concentric Pt ring as counter electrode were employed. A saturated calomel electrode (SCE) was chosen as reference. Test solution was 5 wt% NaCl (analytical-reagent grade) saturated with deoxygenated CO_2. The oxygen concentration of the solution was measured with a DCR OXI200 (Chemetrics®), and it was kept below 40 ppb during the experiments. A positive pressure of deoxygenated CO_2 was maintained throughout the experiments to avoid air ingress. The pH was adjusted to 6 adding 10–15 ml of deoxygenated 1.0 M aq. $NaHCO_3$.

A commercial imidazoline-based product ($R_1 = (CH_2)_n–CH_3$ $n = 10–17$, $R_2 = (CH_2)_2–NH_2$) was used as inhibitor. Following the inhibitor manufacturer specifications, a concentration of 50 ppm was employed.

The inhibitor was added at the beginning of the experiment (non-pre-corroded samples) and after two pre-corrosion periods: 24 and 72 h. During the pre-corrosion period, measurements were taken every 24 h. The formation of the inhibitor film was evaluated after 2 h and subsequently after every 24 h.

The samples were kept at open circuit potential during their exposure to the corrosive medium.

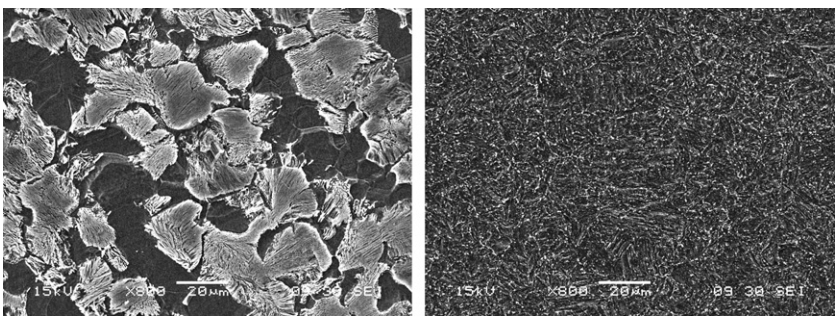

Fig. 1. Microstructures of FP samples (left) and TM samples (right).

A Voltalab PGZ 402 unit was used for electrochemical measurements. EIS was measured at the corrosion potential (E_{corr}) using an applied potential of ±0.005 V rms with a frequency range of 100,000–0.03 Hz. Linear polarization resistance (LPR) was calculated by polarizing the working electrode ±0.015 V vs. E_{corr} with a sweep rate of 10^{-4} V/s. The corrosion potential was also monitored before and after DC and AC analyses.

Potentio-dynamic polarization curves were drawn at the end of the experiments. The sweep rate was 10^{-3} V/s and the scanning range −0.3 V and 0.25 V from E_{corr} for the cathodic and anodic curves, respectively.

The electrochemical data were analyzed by the VoltaMaster 4 and Zview 2 software.

To assess the surface films, a scanning electron microscope (SEM Phillips XL 30) was used. The samples were washed and dried after being withdrawn from the test cell to enable the characterization of adherent corrosion products with no salt residues.

The corrosion rate (C_R) was calculated applying Stearn Geary equation. An approximate value parameter B = 0.017 V was applied [23].

At least six replicas were tested for each experimental condition.

3. Results and discussion

3.1. DC electrochemical results

3.1.1. Linear polarization

Table 1 shows the corrosion rate, R_p and E_{corr} results for both steel microstructures versus the pre-corrosion time without inhibitor addition.

With regard to the microstructure, differences in corrosion rate tendency arose with time. During short exposure periods, specimens with both microstructures behaved similarly, but after 72 h, the corrosion rate was about 20% lower for ferritic–pearlitic microstructure compared to the tempered martensite one.

In order to confirm if the observed changes in corrosion rate between microstructures for different exposure times do not fall into the limits of experimental uncertainty, an ANOVA (Analysis of Variance) test was performed. The analysis showed that corrosion rate variations between microstructures after 24 h of immersion are statistically significant.

Better behaviour of FP samples could be explained by the presence of a $FeCO_3$ protective film, whose precipitation could be favoured by the increase in ferrous ion concentration within the cementite lamellae in the former pearlite colonies. The exposed lamellae were also suggested [11,24] to have an anchoring effect that contributed to film properties improvement.

Tables 2 to 4 list the corrosion rate, R_p and E_{corr} values for non-pre-corroded and pre-corroded samples exposed to the inhibitor.

For all the experimental conditions, the inhibitor moves the corrosion potential towards more positive values, denoting its anodic behaviour.

Moreover, on inhibitor addition, corrosion rate strongly decreases, this effect being dependent on the steel microstructure and the pre-corrosion length.

When non-pre-corroded samples are immersed in an inhibited solution, there is a remarkable decrease in corrosion rate of specimens with both microstructures already in the first 2 h. For longer exposure times, efficiency keeps increasing, but after 72 h, the average corrosion rate of TM samples is 20% smaller than that of FP, thereby demonstrating that the inhibiting effect is better on tempered martensite microstructure.

A beneficial effect is also observed in both microstructures when the inhibitor is added after 24 h of pre-corrosion (Table 3), however, under these experimental conditions, the differences

Table 1
E_{corr}, R_p and C_R. TM and FP samples pre-corroded during 2, 24, 48, and 72 h

Pre-corrosion period (h)	TM			FP		
	E_{corr} (mV/SCE)	R_p (Ω cm^2)	C_R (mm/y)	E_{corr} (mV/SCE)	R_p (Ω cm^2)	C_R (mm/y)
2	−761	139 ± 11	1.4 ± 0.1	−755	140 ± 10	1.4 ± 0.1
24	−751	166 ± 14	1.2 ± 0.1	−747	169 ± 15	1.15 ± 0.1
48	−745	167 ± 18	1.2 ± 0.1	−742	188 ± 20	1.05 ± 0.1
72	−743	159 ± 26	1.25 ± 0.2	−739	191 ± 27	1.05 ± 0.15

Table 2
E_{corr}, R_p and C_R. TM and FP samples non-pre-corroded with 2, 24, 48 and 72 h of exposure to inhibitor

Inhibition period (h)	TM			FP		
	E_{corr} (mV/SCE)	R_p (Ω cm^2)	C_R (μm/y)	E_{corr} (mV/SCE)	R_p (Ω cm^2)	C_R (μm/y)
2	−650	14,763 ± 1118	13.5 ± 1	−659	12,225 ± 2397	16 ± 3
24	−649	41,500 ± 7059	4.5 ± 0.8	−646	38,186 ± 7646	5 ± 0.1
48	−650	54,425 ± 8303	3.5 ± 0.5	−643	43,768 ± 6925	4.5 ± 0.7
72	−656	53,204 ± 12038	3.5 ± 0.8	−649	43,084 ± 4778	4.5 ± 0.5

Table 3
E_{corr}, R_p and C_R. TM and FP samples pre-corroded during 24 h with 2, 24, 48, and 72 h of exposure to inhibitor

Inhibition period (h)	TM			FP		
	E_{corr} (mV/SCE)	R_p (Ω cm^2)	C_R (μm/y)	E_{corr} (mV/SCE)	R_p (Ω cm^2)	C_R (μm/y)
2	−665	2783 ± 904	70 ± 23	−671	1436 ± 224	137 ± 21
24	−638	18814 ± 3536	10 ± 2	−628	11,972 ± 2563	16 ± 3
48	−622	21,707 ± 4275	9 ± 2	−634	16,278 ± 1206	12 ± 1
72	−634	27,179 ± 5972	7 ± 2	−623	17,900 ± 5740	11 ± 3

Table 4
E_{corr}, R_p and C_R. TM and FP samples pre-corroded during 72 h with 2, 24, 48, and 72 h of exposure to inhibitor

Inhibition period (h)	TM			FP		
	E_{corr} (mV/SCE)	R_p (Ω cm^2)	C_R (μm/y)	E_{corr} (mV/SCE)	R_p (Ω cm^2)	C_R (μm/y)
2	−689	940 ± 459	210 ± 102	−698	1062 ± 392	186 ± 68
24	−639	11,007 ± 2950	18 ± 5	−648	10,802 ± 2255	18 ± 4
48	−625	13,023 ± 3633	15 ± 4	−643	14,109 ± 1606	14 ± 2
72	−626	16,224 ± 5589	12 ± 4	−644	13,943 ± 2290	14 ± 2

between both types of samples are greater. At the end of the inhibiting period, the average corrosion rate of TM is about 35% lower than that of FP.

For 72 h of pre-corrosion (Table 4), the inhibitor positive contribution is also detected. The behaviour is similar for both microstructures, but TM samples seem to have a decreasing tendency of corrosion rate with time of inhibition, while FP ones could have attained a steady state. Longer exposure times would be necessary to clarify microstructure influence on this pre-corrosion condition.

Even though the detrimental effect of pre-corrosion is evident, the high efficiency attained by the inhibitor for both microstructures along all pre-corrosion periods is substantial (Tables 1 and 4). Microstructure influence becomes less noticeable for the longest pre-corrosion periods.

The dispersions of polarization resistance (R_p) values are higher for TM than for FP samples, denoting that the film formed on these samples after the inhibitor addition is more sensitive to the minor perturbations of the experimental conditions. Nevertheless, and despite having higher dispersion values, the TM samples behave better under most evaluated conditions.

3.1.2. Polarization curves

When samples are corroded without the inhibitor addition, the anodic polarization curves (Fig. 2) show a Tafel anodic slope within 40 and 60 mV in agreement with other authors results [4,17]. At higher potential, the current rise slows indicating the formation of some corrosion products on the metal surface as reported elsewhere [5]. The main cathodic reactions at pH 6 should be the direct reduction of H_2CO_3 and HCO_3^- (Eqs. (1) and (2)) which are under diffusional control at the corrosion potential (Fig. 2). The polarization curves for TM microstructure behaved just the same.

Fig. 2 also depicts the effect of the inhibitor addition. The inhibitor appears to block anodic and cathodic sites, still this effect is even more significant on non-pre-corroded samples. Besides, the anodic slope increases probably as a consequence of the formation of a surface protective film. It is worth noting that this effect relies on surface conditions. When samples are pre-corroded, anodic slopes are higher than when non-pre-corroded samples are immersed in an inhibited solution. This could be linked to some kind of interaction between corrosion products and inhibitor adsorption and film formation. The change in the cathodic slopes is also dependant on surface conditions. From the preceding, it appears that longer periods of pre-corrosion testing are required to understand this behaviour.

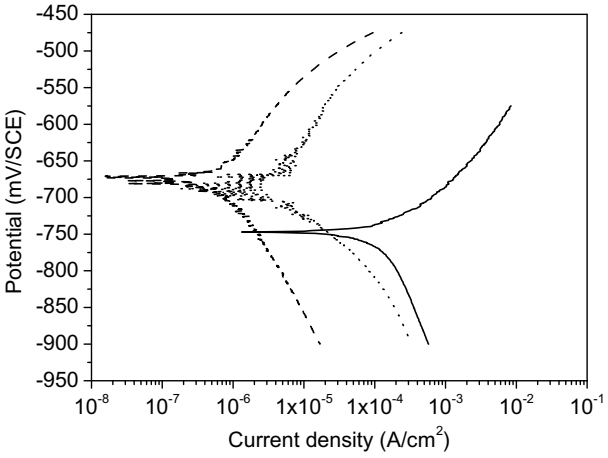

Fig. 2. Polarization curves for FP samples, without inhibitor (—), pre-corroded during 24 h with 24 h of inhibition (·····), and non-pre-corroded samples with 24 h of inhibition (- - -).

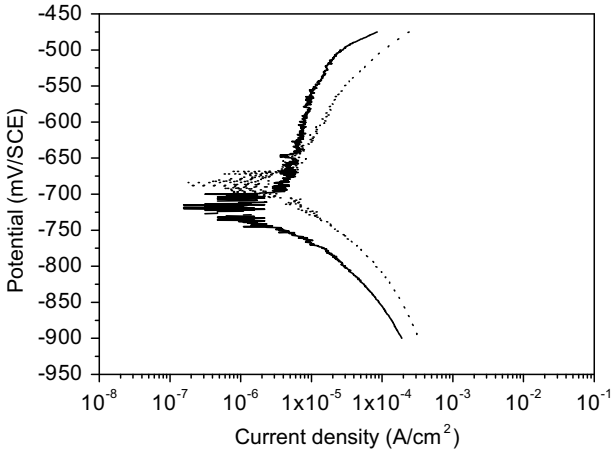

Fig. 3. Comparison between polarization curves of TM (–) and FP (·····) samples pre-corroded during 24 h with 24 h of exposure to inhibitor.

The change of anodic slopes due to the inhibitor addition is microstructure dependent, being higher for TM samples (Fig. 3).

3.2. Surface morphology analysis

A homogeneous attack was observed along the whole surface for all tested specimens. In the case of quenched and tempered samples, corrosion products appear throughout the surface (Fig. 4a). At higher magnification, the presence of carbides can be detected in the corrosion products (Fig. 4e). In the ferritic–pearlitic samples, the microstructure is revealed after corrosion. Ferrite is corroded preferentially, and corrosion products deposited on top of pearlite can be observed (Fig. 4c and f).

After 72 h of inhibition, there is no evidence of a continuous protective film on the pre-corroded sample surfaces, but there seems to be greater built up of corrosion products (Fig. 4b and d) due to the inhibitor action. The possible removal of a protective film formed could have occurred during the sample preparation, prior to corrosion film analysis.

Fig. 5 shows the morphology of surfaces corresponding to non-pre-corroded samples kept in contact with the inhibited solution for 72 h. These samples show no evidence of a homogeneous compact protective film either, but both microstructures remain practically uncorroded, except for a slight corrosion present on some

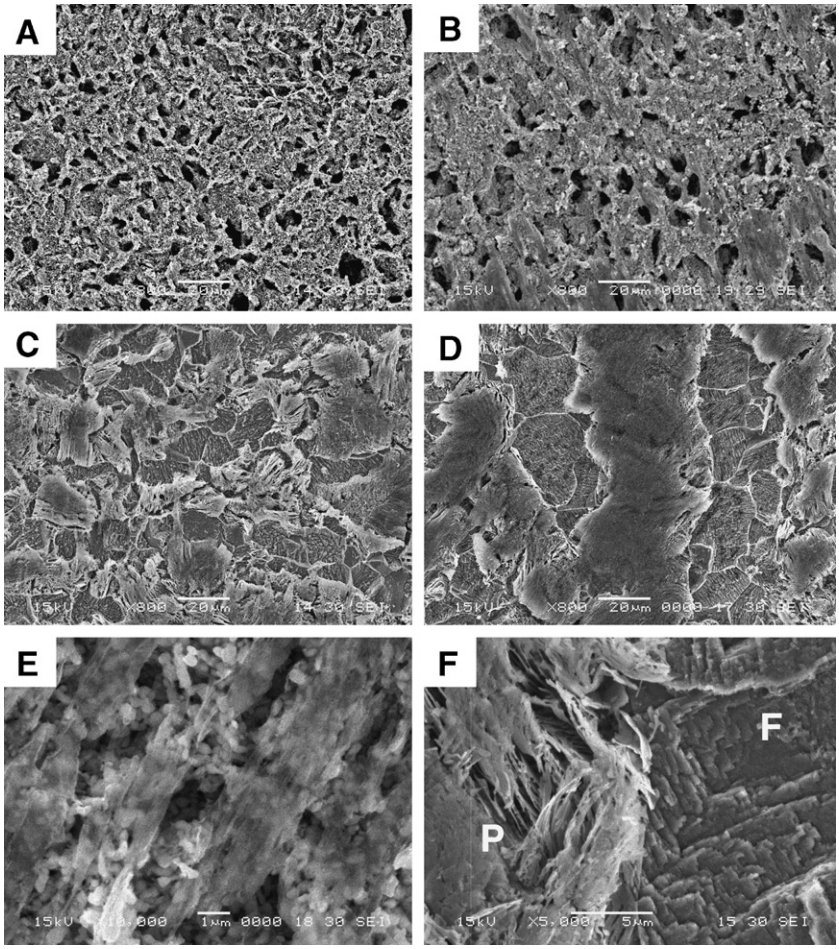

Fig. 4. Corroded surfaces of (A) TM samples pre-corroded for 72 h, (B) TM samples pre-corroded during 72 h with 72 h of inhibition, (C) FP samples pre-corroded during 24 h, (D) FP samples pre-corroded during 24 h with 72 h of inhibition. Detail of the corrosion products of samples corroded during 24 h, (E) TM, (F) FP indications are referred to ferrite and pearlite zones.

part of the surfaces. This is probably originated at the very beginning of the test, before the complete surface coverage by the inhibitor.

SEM images show that there is a modification of corrosion product morphology due to the inhibitor action. These results are in accordance with those obtained previously for imidazoline based inhibitors [19,20]. By means of XPS it was demonstrated that the amount and chemical composition of corrosion products vary with steel microstructure and the molecular structure of the employed inhibitor. Nevertheless no clear evidence of the inhibitor film was found.

3.3. AC electrochemical results

Electrochemical impedance spectra for some of the experimental conditions are shown as Bode plots in Fig. 6.

For samples corroded without the inhibitor addition, only one peak is in the phase angle (α) vs. frequency (f) plot, indicating that there is only one time constant. Such time constant is related to the corrosion processes at the metal/corrosion products/electrolyte interphase, and could be modelled by a simple Randles equivalent circuit (Fig. 7a) that allows electrolyte resistance (R_S), charge transfer resistance (R_{CT}) and double layer capacitance calculation.

When modelling corrosion problems, ideal capacitors are frequently replaced by Constant Phase Elements (CPE) representing leaky or non-ideal capacitors with a view to compensating for non-homogeneity in the system [25]. The impedance of a CPE is described by the expression below:

$$Z_{CPE} = Y^{-1}(i\omega)^{-n} \quad (3)$$

where "Y" is proportional to the capacitance of the corroding system [26], "i" is $\sqrt{-1}$, "ω" is $2\pi f$, and "n" represents a phase shift.

When non-pre-corroded samples are immersed in an inhibited solution, the behaviour after 72 h is quite distinct (Fig. 6). For both microstructures, the impedance module throughout the frequency range is two orders of magnitude higher than that corresponding to those with no inhibitor.

From the α vs. f plot, two separate peaks can be clearly seen indicating the existence of at least two time constants. The high frequency time constant would indicate the presence of a thin isolating and protective inhibitor film covering the surface [27]. The low frequency one could be related to corrosion processes at the unprotected sites of the metal surface as the electrolyte penetrates into the inhibitor film pores. The equivalent electrical circuit shown in Fig. 7b representing a porous inhibitor film formed on the metal surface was proposed to model this behaviour, in which Z_{CPEF} is related to the non-ideal capacitance of the inhibitor film, R_F to the inhibitor film pores resistance, and Z_{CPEdl} to the non-ideal capacitance of the double layer of the electrolyte/corrosion products/metal interphase. As no good fitting was obtained, a new model was considered (Fig. 7c) which yielded very good agreement with the experimental data. This model represents the presence of

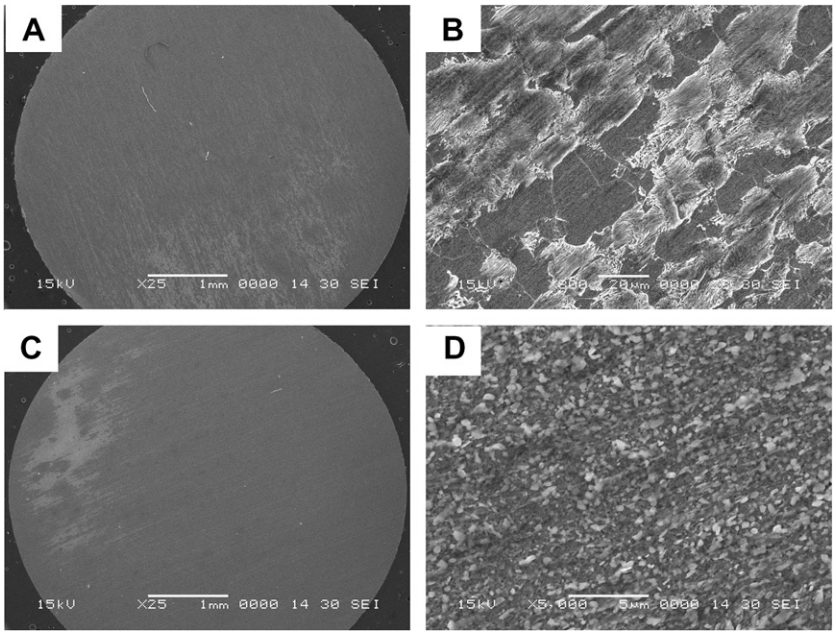

Fig. 5. Surfaces of samples without pre-corrosion exposed to inhibitor during 72 h. General view of the slightly corroded zones on (A) FP samples, (C) TM samples. Detail of the attack on (B) FP samples, (D) TM samples.

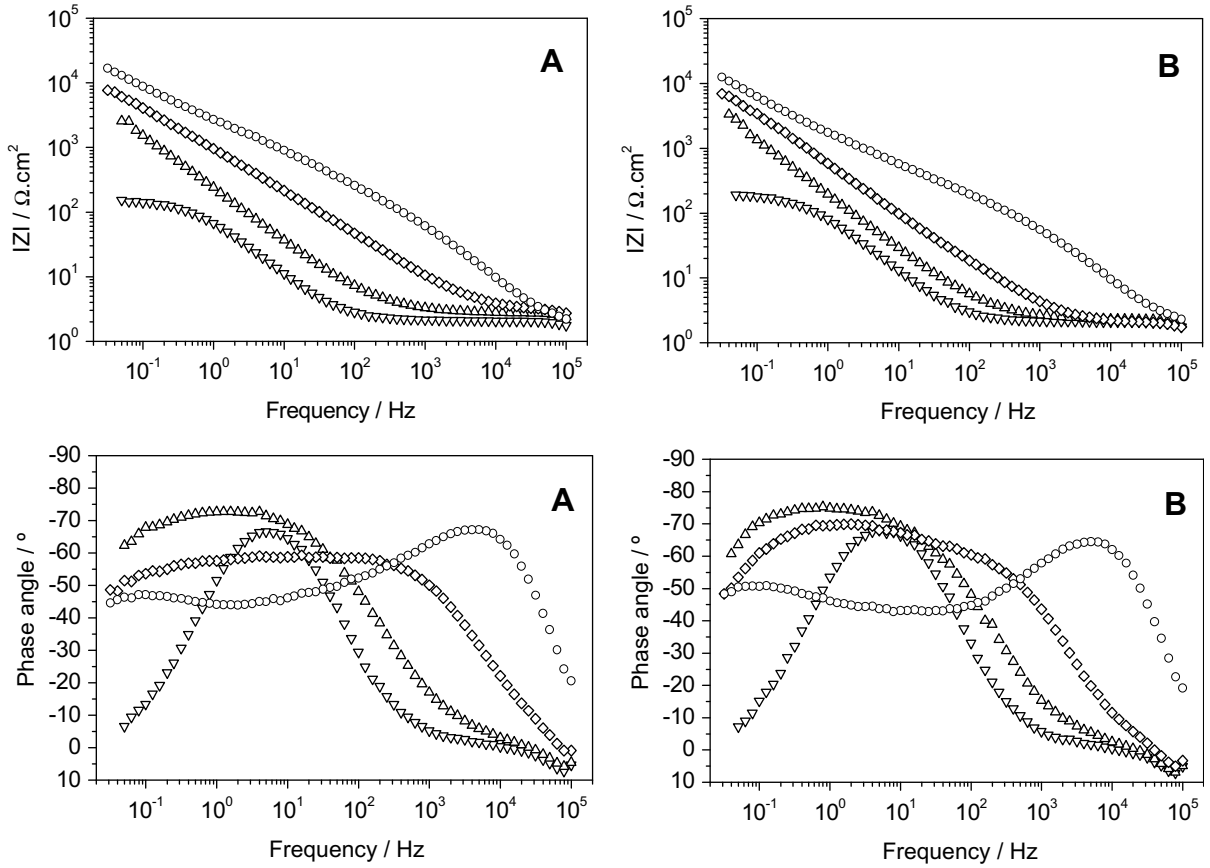

Fig. 6. Bode plots for (A) TM and (B) FP samples, corroded during 72 h (▽), pre-corroded during 72 h with 72 h of inhibition (△), pre-corroded during 24 h with 72 h of inhibition (◇), and without pre-corrosion exposed to inhibitor during 72 h (○).

a porous bilayer inhibitor film: the inner layer is formed on the metal surface and the outer layer on top of the latter, both with different electrical properties. In this equivalent circuit Z_{CPEFO} and R_{FO} and Z_{CPEFI} and R_{FI} are related to the non-ideal capacitance, and to

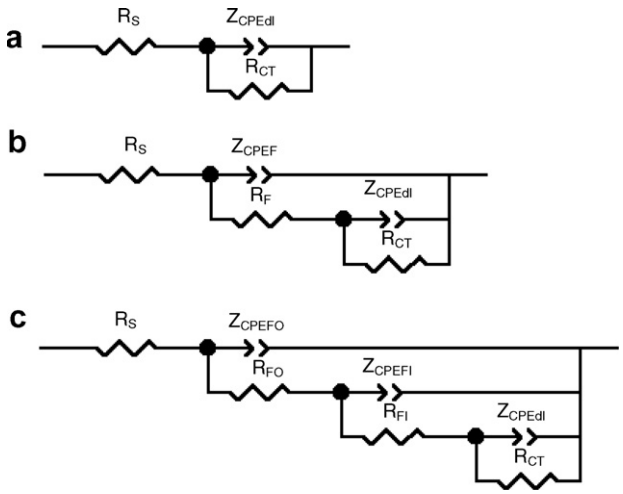

Fig. 7. Different equivalent circuits used for the modelling of the impedance data.

the pores resistance of the outer and inner layer of the inhibitor film, respectively.

For imidazolines based inhibitors, the formation of a multilayer film structure is also proposed by other researchers [28,29].

With regard to samples of both microstructures pre-corroded for 24 h and kept in contact with the inhibitor during 72 h (Fig. 6), two time constants can also be detected in the α vs. f plot. But in comparison with the non-pre-corroded samples spectra, the impedance module values are lower and the high frequency time constant is shifted to lower frequencies, indicating the existence of an inhibitor film with worse properties. This behaviour was successfully modelled with the equivalent circuit shown in Fig. 7b.

After the 72 h of pre-corrosion plus the 72 h of inhibition (Fig. 6), both microstructures show only one time constant, just as in samples corroded without the inhibitor addition. This does not imply the absence of a second time constant since a superimposition with the low frequency one could have occurred, considering their particular electrical properties. The impedance module values are lower than those of samples pre-corroded for 24 h, indicating the detrimental effect surface degradation has. Nevertheless, the beneficial effect of the inhibitor can be clearly appraised if the impedance values are compared with those measured without the inhibitor addition.

Tables 5 to 7 list the circuit parameters corresponding to the modelling of impedance spectra for all the experimental conditions studied. Fitting errors were below 10%.

As mentioned above, when the inhibitor is added to non-pre-corroded samples, the protective film seems to be made up of two layers with different electrical properties. For both microstructures, the inhibitor film is already formed after the first two hours of exposition. The resistance of the inner layer (R_{FI}) is two orders of magnitude higher than that of the outer one (R_{FO}) (Table 5) which would suggest that the number of pores per unit of area and/or the pores size that could be penetrated by the electrolyte is smaller. This could be related to an inner layer higher molecular density as proposed by other authors [28]. The capacitance of the inner layer (Y_{CPEFI}) is higher than that of the outer, and the value of the constant phase element exponent (n_{CPEFI}) is between 0.5 and 0.7. This low value would indicate a strong inhomogeneity in the current flowing through both layers. This could be attributed to an unclearly defined limit between both layers.

Regarding the microstructure, the charge transfer (R_{CT}) and film ($R_{FI} + R_{FO}$) resistances of TM samples are higher even for short periods of exposure (2 h) than those of ferrictic–pearlitic ones, demonstrating that the film formed on quenched and tempered samples has better isolating properties.

As Table 6 shows, the electrical parameters for both microstructures corroded for 24 h without the inhibitor addition are very similar and R_{ct} values agree with the R_p ones obtained from DC experiments. Two hours after the inhibitor addition, the film has not yet developed; but the electrical properties of the double layer have improved. It is also worth noting that the adsorption on TM samples is faster. For longer exposure periods, the formation of an isolating film can be seen for both microstructures. After 72 h, the charge transfer resistance increases more than 10 times if

Table 5
Circuit parameters from the modelling of impedance spectra for non-pre-corroded TM and FP samples exposed to inhibitor

Inhibition period (h)	R_S (Ω cm^2)	Y_{CPEFO} (Ω^{-1} cm^{-2} s^n 10^{-6})	n_{CPEFO}	R_{FO} (Ω cm^2)	Y_{CPEFI} (Ω^{-1} cm^{-2} s^n 10^{-6})	n_{CPEFI}	R_{FI} (Ω cm^2)	Y_{CPEdl} (Ω^{-1} cm^{-2} s^n 10^{-6})	n_{CPEdl}	R_{CT} (Ω cm^2)
TM – without pre-corrosion										
2	2.5	1.6	1	35	100	0.54	5889	81	0.68	7191
72	2.7	1.3	1	55	103	0.53	9552	41	0.78	77,039
FP – without pre-corrosion										
2	2.5	1.6	1	21	61	0.68	1507	202	0.64	8380
72	2.3	1.9	1	44	125	0.54	2274	131	0.79	71,009

Table 6
Circuit parameters from the modelling of impedance spectra for TM and FP samples pre-corroded during 24 h with posterior exposition to inhibitor

	R_S (Ω cm^2)	Y_{CPEF} (Ω^{-1} cm^{-2} s^n 10^{-6})	n_{CPEF}	R_F (Ω cm^2)	Y_{CPEdl} (Ω^{-1} cm^{-2} s^n 10^{-6})	n_{CPEdl}	R_{CT} (Ω cm^2)
TM							
24 h pre-corrosion	2.3	–	–	–	1353	0.85	164
Inhibition period (h)							
2	3.2	–	–	–	904	0.8	2386
72	2.9	143	0.76	125	180	0.56	49330
FP							
24 h pre-corrosion	2.2	–	–	–	1391	0.86	167
Inhibition period (h)							
2	2.1	–	–	–	1157	0.82	1321
72	2	287	0.8	77	109	0.78	17869

Table 7
Circuit parameters from the modelling of impedance spectra for TM and FP samples pre-corroded during 72 h with posterior exposition to inhibitor

	R_S (Ω cm^2)	Y_{CPEdl} (Ω^{-1} cm^{-2} s^n 10^{-6})	n_{CPEdl}	R_{CT} (Ω cm^2)
TM				
72 h pre-corrosion	2.1	2535	0.87	153
Inhibition period (h)				
2	2.1	1926	0.84	970
72	2.8	934	0.81	16,229
FP				
72 h pre-corrosion	2.1	2131	0.87	195
Inhibition period (h)				
2	2.2	1814	0.87	1035
72	2.4	1071	0.83	13,979

compared to that at 2 h of exposure, again being higher for TM samples. The film pores resistance (R_F) is also higher, and the film capacitance (Y_{CPEF}) is lower for quenched and tempered samples, indicating that the film formed on these specimens has better protective properties than that formed on FP ones.

For 72 h of pre-corrosion (Table 7), ferritic–pearlitic samples show a slightly smaller double layer capacitance (Y_{CPEdl}) and a higher charge transfer resistance (R_{CT}). This is in accordance with the lower corrosion rate values obtained from DC experiments. When the inhibitor is added, both microstructures show a significant increase in the charge transfer resistance and a decrease in the double layer capacitance; this effect is more noticeable for longer contact periods with the inhibitor. After 72 h of inhibition, the charge transfer resistance is two orders of magnitude higher than that of non-inhibited samples. Once again TM samples provided a better performance.

The above results confirm that the inhibitor behaves better on non-corroded surfaces, and that this effect is microstructure dependent. The differences between the tempered martensite and the ferritic–pearlitic specimens on the adsorption and formation of the inhibitor film could be related to their very different superficial iron carbide distribution (Fig. 1). Considering that the inhibitor will be more strongly adsorbed through Lewis acid–base interactions with the exposed Fe_3C compared to metallic iron and ferrous ions [22], the morphology and distribution of these iron carbides should not be overlooked.

Even though other authors have also determined the detrimental influence of pre-corrosion on inhibitors efficiency [18,30] the proposed mechanism is related to the accumulation of laminar cementite on the steel corroded surface which provides a larger cathodic area. The results described above do not entirely support this mechanism because the pre-corrosion effect is present in both microstructures. Even the one with less cementite accumulation on surface (TM) [19] is sensitive to this effect.

The detrimental effect of pre-corrosion on the inhibitor film formation could be related to at least two distinct causes. On the one hand, as there are different compounds (α-Fe, Fe_3C, $FeCO_3$) on the corroded surface, the properties of the inhibitor adsorption could be different on each of them. On the other hand, the more intricate surface resulting from the corrosion process before the inhibitor addition, makes it more difficult for the inhibitor molecules to displace water and reach the reaction sites. Regardless of the cause, the resulting film will tend to form more slowly and be more defective.

Further research should be conducted in order to provide more evidence on the effect of the microstructure and characteristics of corrosion products films on inhibition mechanisms. Particularly, regarding the influence of cementite accumulation on the surface, it would be very useful to monitor the system for longer pre-corrosion and inhibition periods.

4. Conclusions

The following conclusions can be drawn from the results above:

1. For both microstructures, a protective film that greatly decreases the corrosion rate is formed after the inhibitor addition under all tested conditions.
2. Pre-corrosion has a negative effect on the inhibitor efficiency for both microstructures.
3. Steel microstructure affects the inhibitor performance, and the inhibitor films formed on Q & T samples proved to be better under most experimental conditions tested.

Acknowledgements

This work was supported by the Argentine Research Council for Science and Technology (CONICET), TENARIS- SIDERCA and by the University of Mar del Plata.

References

[1] M.B. Kermani, A. Morshed, Carbon dioxide corrosion in oil and gas production – A compendium, Corrosion 59 (2003) 659–683.
[2] D.A. Lopez, T. Perez, S.N. Simison, The influence of microstructure and chemical composition of carbon and low alloy steels in CO_2 corrosion. A state-of-the-art appraisal, Mater. Des. 24 (2003) 561–575.
[3] S. Nesic, J. Postlethwaite, S. Olsen, An electrochemical model for prediction of corrosion of mild steel in aqueous carbon dioxide solutions, Corrosion 52 (1996) 280–294.
[4] M. Nordsveen, S. Nesic, R. Nyborg, A. Stangeland, A mechanistic model for carbon dioxide corrosion of mild steel in the presence of protective iron carbonate films – Part 1: Theory and verification, Corrosion 59 (2003) 443–456.
[5] B.R. Linter, G.T. Burstein, Reactions of pipeline steels in carbon dioxide solutions, Corros. Sci. 41 (1999) 117–139.
[6] S. Nesic, K.L.J. Lee, A mechanistic model for carbon dioxide corrosion of mild steel in the presence of protective iron carbonate films – Part 3: Film growth model, Corrosion 59 (2003) 616–628.
[7] K. Videm, A. Dugstad, Corrosion of carbon–steel in an aqueous carbon-dioxide environment. Part 1: solution effects, Mater. Perform. 28 (1989) 63–67.
[8] K. Videm, A. Dugstad, Corrosion of carbon–steel in an aqueous carbon-dioxide environment. 2. Film formation, Mater. Perform. 28 (1989) 46–50.
[9] M. Ueda, H. Takabe, Effect of environmental factor and microstructure on morphology of corrosion products in CO_2 environments, Proc. NACE Corros. 99 (1999) (Paper No. 13).
[10] J.K. Heuer, J.F. Stubbins, An XPS characterization of $FeCO_3$ films from CO_2 corrosion, Corros. Sci. 41 (1999) 1231–1243.
[11] A. Dugstad, H. Hemmer, M. Seiersten, Effect of steel microstructure upon corrosion rate and protective iron carbonate film formation, Proc. NACE Corros. 2000 (2000) (Paper No. 24).
[12] Handbook of Chemistry and Physics, 79th ed., CRC Press, Boca Raton, FL, USA, 1999.
[13] J.L. Crolet, N. Thevenot, S. Nesic, Role of conductive corrosion products in the protectiveness of corrosion layers, Corrosion 54 (1998) 194–203.
[14] I.L. Rozenfeld, D.B. Bogomolov, A.E. Gorodetskii, L.P. Kazanskii, L.V. Frolova, L.I. Shamova, Formation of protective films on iron under the influence of the inhibitor ifkhangaz-1 in aqueous-solution saturated with hydrogen-sulfide, Protect. Met. 18 (1982) 121–125.
[15] E.C. French, R.L. Martin, J.A. Dougherty, Review of corrosion-inhibitors for gas-wells, Mater. Perform. 28 (1989) 46–49.
[16] L.J. Oblonsky, G.R. Chesnut, T.M. Devine, Adsorption of octadecyldimethylbenzylammonium chloride to two carbon–steel microstructures as observed with surface-enhanced Raman-spectroscopy, Corros. Sci. 51 (1995) 891–900.
[17] E. Gulbrandsen, S. Nesic, A. Stageland, T. Burchardt, S. Sundfaer, S.M. Hesjevik, S. Skjerve, Effect of precorrosion on the performance of inhibitors for CO_2 corrosion of carbon steel, Proc. NACE Corros. 98 (1998) 13.
[18] E. Gulbrandsen, R. Nyborg, T. Loland, K. Nisancioglu, Effect of steel microstructure and composition on inhibition of CO_2 corrosion, Proc. NACE Corros. 2000 (2000) (Paper No. 23).
[19] D.A. Lopez, W.H. Schreiner, S.R. de Sanchez, S.N. Simison, The influence of carbon steel microstructure on corrosion layers – An XPS and SEM characterization, Appl. Surf. Sci. 207 (2003) 69–85.
[20] D.A. Lopez, W.H. Schreiner, S.R. de Sanchez, S.N. Simison, The influence of inhibitors molecular structure and steel microstructure on corrosion layers in

CO_2 corrosion: An XPS and SEM characterization, Appl. Surf. Sci. 236 (2004) 77–97.
[21] D.A. Lopez, S.N. Simison, S.R. de Sanchez, The influence of steel microstructure on CO_2 corrosion. EIS studies on the inhibition efficiency of benzimidazole, Electrochim. Acta 48 (2003) 845–854.
[22] D.A. Lopez, S.N. Simison, S.R. de Sanchez, Inhibitors performance in CO_2 corrosion: EIS studies on the interaction between their molecular structure and steel microstructure, Corros. Sci. 47 (2005) 735–755.
[23] D.A. Jones, Principles and Prevention of Corrosion, Macmillan Publishing Company, 1991.
[24] C.A. Palacios, J.R. Shadley, Characteristics of corrosion scales on steels in a CO_2 – saturated Nacl brine, Corrosion 47 (1991) 122–127.
[25] ZPlot for Windows, Electrochemical Impedance Software Operating Manual, Version 2.1, Scribner Associates Inc., 1998.
[26] C.H. Hsu, F. Mansfeld, Technical note: concerning the conversion of the constant phase element parameter Y-0 into a capacitance, Corrosion 57 (2001) 747–748.
[27] C.H. Tsai, F. Mansfeld, Determination of coating deterioration with EIS: Part II. development of a method for field testing of protective coatings, Corrosion 49 (1993) 726–737.
[28] Y.J. Tan, S. Bailey, B. Kinsella, An investigation of the formation and destruction of corrosion inhibitor films using electrochemical impedance spectroscopy (EIS), Corros. Sci. 38 (1996) 1545–1561.
[29] S. Ramachandran, V. Jovancicevic, Molecular modeling of the inhibition of mild steel carbon dioxide corrosion by imidazolines, Corrosion 55 (1999) 259–267.
[30] J.L. Mora-Mendoza, S. Turgoose, Fe_3C influence on the corrosion rate of mild steel in aqueous CO_2 systems under turbulent flow conditions, Corros. Sci. 44 (2002) 1223–1246.